A Cosserat rod model with microstructure

New Journal of Physics
The open-access journal for physics

A Cosserat rod model with microstructure

Tim Gould[1] **and David A Burton**

Department of Physics, Lancaster University, Lancaster LA1 4YB, UK
E-mail: t.gould@lancaster.ac.uk

New Journal of Physics **8** (2006) 137
Received 13 February 2006
Published 18 August 2006
Online at http://www.njp.org/
doi:10.1088/1367-2630/8/8/137

Abstract. A novel continuum mechanical model of long, flexible, hollow tubes is developed using the Cosserat theory of rods and used to study the mechanics of carbon nanotubes. By adding 'microstructure' to a Cosserat rod, analyses of tubes with deformable cross-sections are permitted. To facilitate the analysis, an approximation is introduced that reduces the infinite number of microstructural degrees of freedom to one complex scalar field. The Cosserat rod and microstructure system is solved both numerically and analytically.

Contents

[1] Author to whom any correspondence should be addressed.

PII: S1367-2630(06)18740-6

1. Introduction

Much study has been given to the behaviour of long, flexible structures (often termed rods). The Cosserat rod model (see [1]) is a powerful, continuum-based approach for modelling the behaviour of rods under a wide variety of external stimuli and conditions through a simple set of coupled two-dimensional, second order, nonlinear partial differential equations (PDEs).

While the Cosserat rod approach is highly versatile it is limited to modelling slender structures whose cross-sections are essentially rigid. For example, in many cases the cross-sections of bent hollow tubes adopt shapes that are substantially different from their unstrained state. One possibility is to model the hollow tube using a Cosserat shell theory [1]. The principal disadvantage of the Cosserat shell approach (in comparison to a Cosserat rod theory) is that it is formulated using a system of three-dimensional PDEs, whereas a Cosserat rod theory only employs two-dimensional PDEs. In the former case the independent variables include two spatial degrees of freedom (and one temporal) whereas in the latter case they include only one spatial degree of freedom (and one temporal). Hence, a *static* Cosserat rod satisfies a system of *ordinary* differential equations (ODEs) and enjoys all of the inherent computational and analytical advantages that ODEs have over PDEs.

With this in mind, a new approach is proposed that builds on Cosserat rod theory and permits dynamical analyses of hollow tubes whose cross-sections are deformable. The degrees of freedom describing the deformations of the cross-sections model the 'microstructure' of the hollow tube, i.e. deformations of the surface of the tube that cannot be described using standard Cosserat rod theory. Unlike Cosserat shell theory the static states of the new theory satisfy ODEs.

2. Limitations of Cosserat rod theory

A necessary ingredient in any continuum mechanical theory of a *hollow tube* (from now on, simply described as a *tube*) is its undeformed (reference) state, which is assumed to be uniform. The reference state is characterized by the following constants: L is the length of the tube, R the diameter of the (uniform) cross-section, a the (uniform) 'thickness' of the cylinder and ρ the (uniform) density of the material. The stresses associated with deformations of the tube are formulated using the elastic modulus E and shear modulus G. It assumed below that $L^2 \gg R^2$ and $R^2 \gg a^2$. Figure 1 shows the essential structure of such a tube.

A Cosserat rod is described by a one-to-one mapping $\boldsymbol{\Phi}$ from a reference configuration in $\mathbb{R}^3$ to a deformed configuration in $\mathbb{R}^3$. Each configuration is coordinated by slicing it into a series of rigid cross-sections. At time t each material point is labelled uniquely by the triple (s, x, y) where s labels each cross-section uniquely and (x, y), at fixed s, uniquely labels the material points within the cross-section s. The mapping $\boldsymbol{\Phi}$ is written as [2]

$$\boldsymbol{\Phi}(s, x, y, t) := \boldsymbol{r}(s, t) + \sum_{\alpha} \zeta_\alpha(x, y)\boldsymbol{d}_\alpha(s, t) \tag{1}$$

where $\boldsymbol{r}(s, t)$ is the position of a representative point in the cross-section s at time t. The pair of vectors $\boldsymbol{d}_\alpha(s, t)$ is a basis for locating material points in the cross-section s at time t. The orthonormal 'director' frame $(\boldsymbol{d}_1, \boldsymbol{d}_2, \boldsymbol{d}_3 = \boldsymbol{d}_1 \times \boldsymbol{d}_2)$ is written as the rotation of the

[2] Unless otherwise specified, lowercase Latin indices run over 1, 2, 3, while lowercase Greek indices run over 1, 2.

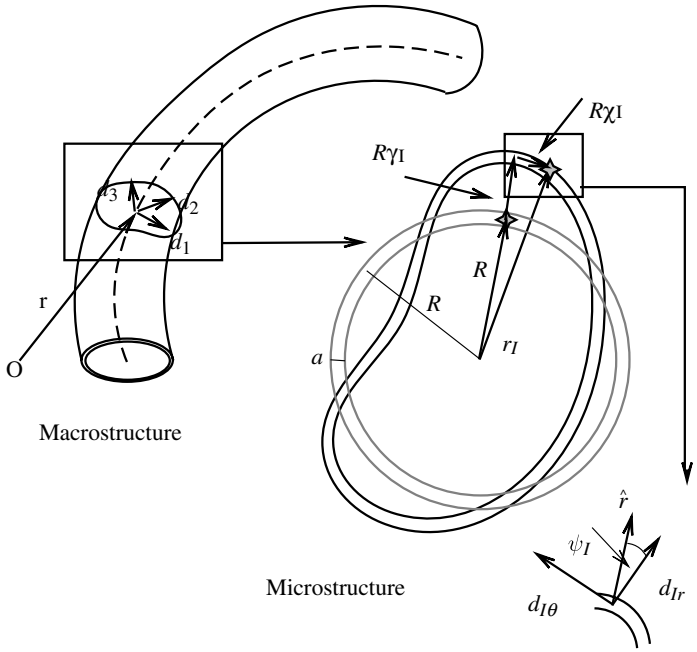

Figure 1. Diagram of a Cosserat rod with microstructure. The stars label the same material point in two different configurations.

inertial Cartesian frame $(\boldsymbol{e}_1, \boldsymbol{e}_2, \boldsymbol{e}_3)$ whose axis is $\hat{\boldsymbol{\phi}}$ and whose magnitude is $|\boldsymbol{\phi}|$ radians. Thus, $\boldsymbol{d}_i \cdot \boldsymbol{d}_j = \boldsymbol{e}_i \cdot \boldsymbol{e}_j = \delta_{ij}$ where δ_{ij} is the Kronecker delta.[3] Associated with any vector $\boldsymbol{x}$ is the dual vector $\tilde{\boldsymbol{x}}$ (covector) defined as the linear mapping $\tilde{\boldsymbol{x}}(\boldsymbol{y}) \equiv \boldsymbol{x} \cdot \boldsymbol{y}$ over all vectors $\boldsymbol{y}$. Linear maps on vectors and covectors written $\boldsymbol{T} = \sum_{ij} \boldsymbol{x}_i \otimes \tilde{\boldsymbol{y}}_j$ are type (1,1) tensors where $\boldsymbol{T}(\tilde{\boldsymbol{z}}_1, \boldsymbol{z}_2) = \sum_{ij} (\tilde{\boldsymbol{z}}_1(\boldsymbol{x}_i))(\tilde{\boldsymbol{y}}_j(\boldsymbol{z}_2)) = \sum_{ij} (\boldsymbol{z}_1 \cdot \boldsymbol{x}_i)(\boldsymbol{z}_2 \cdot \boldsymbol{y}_j)$ for any covector $\tilde{\boldsymbol{z}}_1$ and vector $\boldsymbol{z}_2$. Using $\boldsymbol{\phi} = |\boldsymbol{\phi}|\hat{\boldsymbol{\phi}}, \boldsymbol{d}_i(s,t) = \boldsymbol{D}(\boldsymbol{\phi}(s,t))\boldsymbol{e}_i$ where $\boldsymbol{D}(\boldsymbol{\phi}) = \sum_i \boldsymbol{d}_i \otimes \tilde{\boldsymbol{e}}_i = \exp(\boldsymbol{A}(\boldsymbol{\phi}))$ is an element of SO(3) (i.e. an orthonormal transformation) and[4] $\boldsymbol{A}(\boldsymbol{\phi}) = \sum_{ijk} \epsilon_{ijk} \phi_k \boldsymbol{e}_i \otimes \tilde{\boldsymbol{e}}_j$ is an element of $\mathfrak{so}(3)$ where $\boldsymbol{\phi} = \sum_i \phi_i \boldsymbol{e}_i$. Readers are directed to section 2 of [2] for more detail on this approach to Cosserat modelling.

Since the cross-sections are rigid the configuration of the rod is specified entirely by $(\boldsymbol{r}, \boldsymbol{d}_\alpha)$. Integral equations describing the balance of linear and angular momentum are used to obtain PDEs for $(\boldsymbol{r}, \boldsymbol{d}_\alpha)$ in s and t; the functions ζ_α are integrated out leaving functions of s and t only [1].

Cosserat rod theory is an excellent approximation under most circumstances, particularly when dealing with solid rods. However, it is too inaccurate for modelling hollow tubes whose cross-sections are likely to deform considerably under stress. A natural approach to follow for modelling such continua is to use shell theory. For simplicity, we will consider only *static* configurations and omit t (with the exception of work in appendix B where t briefly appears).

The material points in a two-dimensional surface describing a hollow tube are labelled by the pair (s, θ) where s labels the cross-section and θ is an angle around the tube. The location of

[3] $\delta_{ij=1}$ if $i = j$ and $\delta_{ij} = 0$ otherwise.

[4] The Levi-Civita alternative symbol $\epsilon_{ijk} = 1$ if ijk is an even permutation of 123, $\epsilon_{ijk} = -1$ if ijk is an odd permutation of 123 and $\epsilon_{ijk} = 0$ otherwise.

the material point (s, θ) is given as

$$\boldsymbol{\Phi}(s, \theta) := \boldsymbol{r}(s) + \sum_{\alpha} \xi_{\alpha}(s, \theta)\boldsymbol{d}_{\alpha}(s) \tag{2}$$

or

$$\boldsymbol{\Phi}(s, \theta) := \boldsymbol{r}(s) + R((1 + \gamma(\theta, s))\hat{\boldsymbol{r}}(\theta, s) + \chi(\theta, s)\hat{\theta}(\theta, s)) \tag{3}$$

where

$$\hat{\boldsymbol{r}}(\theta, s) = \cos(\theta)\boldsymbol{d}_1(s) - \sin(\theta)\boldsymbol{d}_2(s) \tag{4}$$

$$\hat{\theta}(\theta, s) = \sin(\theta)\boldsymbol{d}_1(s) + \cos(\theta)\boldsymbol{d}_2(s) \tag{5}$$

are radial and angular directions in the cross-section labelled by s. The additional terms $\gamma(\theta, s)$ and $\chi(\theta, s)$ are local deformations (from a circle) of cross-section s in the radial and angular directions and model the microstructure of the tube. The curve $\boldsymbol{r}$ is chosen so that the first area moments of each cross-section vanish.

The reference state of a uniform hollow tube is characterized by the following constants: L is the length of the tube and $s \in [0, L]$, R the diameter of the (uniform) cross-section, a is the (uniform) 'thickness' of the cylinder and ρ is the (uniform) density of the material. The stresses associated with deformations of the tube are formulated using the constant elastic modulus E and constant shear modulus G. It assumed below that $L^2 \gg R^2$ and $R^2 \gg a^2$. Figure 1 shows the essential structure of such a tube.

3. Energy functional of a rod with microstructure

The principal difference between the model developed here and a shell theory is in the formulation of their constitutive responses. In our model the cross-sections remain planar and derivatives with respect to s and θ in the elastic potential energy do not mix. This approach is a powerful alternative to existing methods (for example [3]) for modelling multiwall carbon nanotubes. In such circumstances it is straightforward to devise a model to deal with the inter-tube and intra-tube interactions in a more physically acceptable fashion than [3], possibly employing an effective thickness as proposed in [4].

3.1. Deformation energy of a cross-section

If we deform the cross-sections of a hollow tube, we expect to see a change in the tube's elastic potential energy. An expression for the tube's elastic potential energy is obtained by slicing the tube into a series of N rings, indexed by I, and modelling each ring with standard Cosserat rod theory (a 'rod theory on rod theory' approach).

Following the details of appendix A, we see that the potential energy per unit length $\mathcal{V}_I$ of ring I described by Ψ_I where

$$\Psi_I(\theta, \xi_{Ir}, \xi_{I\theta}) := \boldsymbol{r}_I(\theta) + \xi_{Ir}\boldsymbol{d}_{Ir}(\theta) + \xi_{I\theta}\boldsymbol{d}_{I\theta}(\theta) \tag{6}$$

$$\boldsymbol{r}_I(\theta) = R((1 + \gamma_I(\theta))\hat{\boldsymbol{r}}_I(\theta) + \chi(\theta)\hat{\theta}_I(\theta)) \tag{7}$$

$$\boldsymbol{d}_{Ir}(\theta) = \cos(\psi_I(\theta))\hat{\boldsymbol{r}}_I(\theta) - \sin(\psi_I(\theta))\hat{\theta}_I(\theta) \tag{8}$$

$$\boldsymbol{d}_{I\theta}(\theta) = \sin(\psi_I(\theta))\hat{\boldsymbol{r}}_I(\theta) + \cos(\psi_I(\theta))\hat{\theta}_I(\theta) \tag{9}$$

$$\boldsymbol{d}_{I3} = \boldsymbol{e}_3 \tag{10}$$

is[5]

$$\mathcal{V}_I[\gamma_I, \chi_I, \psi_I] = \pi a R \int_0^{2\pi} \left(\boldsymbol{y}_I \boldsymbol{K}_I \boldsymbol{y}_I + \frac{a^2 E}{12R^2} (\partial_\theta \psi_I(\theta))^2 \right) \mathrm{d}\theta \tag{11}$$

$$\boldsymbol{y}_I = [\partial_\theta \gamma_I(\theta) - \chi_I(\theta) + \sin(\psi_I(\theta))]\hat{\boldsymbol{r}}_I + [\partial_\theta \chi_I(\theta) + \gamma_I(\theta) + 1 - \cos(\psi_I(\theta))]\hat{\theta}_I \tag{12}$$

$$\begin{aligned}\boldsymbol{K}_I = {} & \tfrac{1}{2}(G+E) + \tfrac{1}{2}(G-E)\cos(2\psi_I(\theta))(\hat{\boldsymbol{r}}_I \otimes \tilde{\hat{\boldsymbol{r}}}_I - \hat{\theta}_I \otimes \tilde{\hat{\theta}}_I) \\ & + \tfrac{1}{2}(G-E)\sin(2\psi_I(\theta))(\hat{\boldsymbol{r}}_I \otimes \tilde{\hat{\theta}}_I + \hat{\theta}_I \otimes \tilde{\hat{\boldsymbol{r}}}_I).\end{aligned} \tag{13}$$

Since a tube can be constructed out of a series of rings, each with its own shape defined by Ψ_I, we write the elastic energy of the tube associated with cross-sectional deformations as

$$\mathcal{U}_{\text{tube}} = \sum_{I=1}^{N} \mathcal{V}_I[\gamma_I, \chi_I, \psi_I] h_I \tag{14}$$

where h_I is the height of ring I. In the limit $h_I \to 0$ the sum becomes an integral and the index I is replaced by the variable s so that

$$\mathcal{U}_{\text{tube}} = \int_0^L \mathcal{V}[\gamma, \chi, \psi](s)\, \mathrm{d}s \tag{15}$$

$$= \pi a R \int_0^L \int_0^{2\pi} \left(\boldsymbol{y}(s) \boldsymbol{K}(s) \boldsymbol{y}(s) + \frac{a^2 E}{12R^2} (\partial_\theta \psi(s, \theta))^2 \right) \mathrm{d}\theta\, \mathrm{d}s. \tag{16}$$

3.2. Total elastic energy

The total elastic energy of the tube is given by the sum of $\mathcal{U}_{\text{tube}}$ and a contribution due to the 'bulk' bending, shearing and twisting of the tube. Choosing a Kirchoff-like constitutive relation for the bulk deformations leads to a total elastic energy V of the form

$$V = \int_0^L \int_{\mathcal{C}[\gamma,\chi](s)} \left\{ \sum_\alpha \tfrac{1}{2}\hat{G}(s,\theta)(\partial_s \Phi \cdot \boldsymbol{d}_\alpha)^2 + \tfrac{1}{2}\hat{E}(s,\theta)(\partial_s \Phi \cdot \boldsymbol{d}_3 - 1)^2 \right\} \mathrm{d}A\, \mathrm{d}s + \mathcal{U}_{\text{tube}}[\gamma, \chi, \psi] \tag{17}$$

[5] Let $\boldsymbol{x}$ and $\boldsymbol{y}$ be vectors and $\boldsymbol{T} = \sum_{ij} T_{ij} \boldsymbol{d}_i \otimes \tilde{\boldsymbol{d}}_j$ be a rank 2 tensor. We use the notation $\boldsymbol{x}\boldsymbol{T}\boldsymbol{y} = T(\tilde{\boldsymbol{x}}, \boldsymbol{y})$, i.e. if $\boldsymbol{T} = \sum_{ij} T_{ij} \boldsymbol{d}_i \otimes \tilde{\boldsymbol{d}}_j$, $\boldsymbol{x} = \sum_i x_i \boldsymbol{d}_i$ and $\boldsymbol{y} = \sum_i y_i \boldsymbol{d}_i$ then $\boldsymbol{x}\boldsymbol{T}\boldsymbol{y} = \sum_{ij} x_i M_{ij} y_j$.

where $\alpha = 1, 2$ and $\hat{G}(s, \theta)$ and $\hat{E}(s, \theta)$ are defined such that integrals over the cross-section $\mathcal{C}[\gamma, \chi](s)$ are:

$$\int_{\mathcal{C}[\gamma,\chi](s)} f\hat{G}(s,\theta)\,\mathrm{d}A = aRG\left(\int_0^{2\pi} f\,\mathrm{d}\theta + O(a^2/R^2)\right)$$
$$\int_{\mathcal{C}[\gamma,\chi](s)} f\hat{E}(s,\theta)\,\mathrm{d}A = aRE\left(\int_0^{2\pi} f\,\mathrm{d}\theta + O(a^2/R^2)\right)$$

where f is a function on $\mathbb{R}^3$, a is the thickness and R the reference radius of the tube. Evaluating the area integral gives

$$V = \int_0^L \{\tfrac{1}{2}(\boldsymbol{v}(s) - \boldsymbol{d}_3)\boldsymbol{K}(s)(\boldsymbol{v}(s) - \boldsymbol{d}_3) + \tfrac{1}{2}\boldsymbol{u}(s)\boldsymbol{J}(s)\boldsymbol{u}(s) + \boldsymbol{u}(s)\cdot\boldsymbol{d}_3(s)T[\gamma,\chi](s) + D[\gamma,\chi](s)\}\mathrm{d}s + \mathcal{U}_{\text{tube}}[\gamma,\chi,\psi] \tag{18}$$

where

$$\boldsymbol{v}(s) = \partial_s \boldsymbol{r}(s), \qquad \boldsymbol{u}(s)\times\boldsymbol{d}_i = \partial_s \boldsymbol{d}_i, \tag{19}$$

$$\gamma'(s,\theta) = \partial_s\gamma(s,\theta), \tag{20}$$

$$\chi'(s,\theta) = \partial_s\chi(s,\theta). \tag{21}$$

Here we have chosen $\boldsymbol{r}$ such that the first-moments of area are always zero. As such $\boldsymbol{K}$ and $\boldsymbol{J}$ are similar to their counterparts in standard Cosserat rod theory

$$\boldsymbol{K} = \mathcal{A}(s)(G\boldsymbol{d}_1\otimes\tilde{\boldsymbol{d}}_1 + G\boldsymbol{d}_2\otimes\tilde{\boldsymbol{d}}_2 + E\boldsymbol{d}_3\otimes\tilde{\boldsymbol{d}}_3), \tag{22}$$

$$\boldsymbol{J} = (\mathcal{I}_{11}(s)E\boldsymbol{d}_1\otimes\tilde{\boldsymbol{d}}_1 + \mathcal{I}_{22}(s)E\boldsymbol{d}_2\otimes\tilde{\boldsymbol{d}}_2 + \mathcal{I}_{33}(s)G\boldsymbol{d}_3\otimes\tilde{\boldsymbol{d}}_3) + \mathcal{I}_{12}(s)E(\boldsymbol{d}_1\otimes\tilde{\boldsymbol{d}}_2 + \boldsymbol{d}_2\otimes\tilde{\boldsymbol{d}}_1) \tag{23}$$

but with area moments that depend on s through γ and χ. As an abbreviation we have written $\mathcal{I}_{ij}$ instead of $\mathcal{I}_{ij}[\gamma, \chi]$ (likewise for $\mathcal{A}$) in the above equations. These area moments take the form

$$\mathcal{A}[\gamma,\chi](s) = \int_{\mathcal{C}[\gamma,\chi](s)} \mathrm{d}A \tag{24}$$

$$\mathcal{I}_{11}[\gamma,\chi](s) = \mathcal{M}_{22}[\gamma,\chi](s), \tag{25}$$

$$\mathcal{I}_{22}[\gamma,\chi](s) = \mathcal{M}_{11}[\gamma,\chi](s), \tag{26}$$

$$\mathcal{I}_{12}[\gamma,\chi](s) = \mathcal{M}_{12}[\gamma,\chi](s), \tag{27}$$

$$\mathcal{I}_{33}[\gamma,\chi](s) = \mathcal{M}_{11}[\gamma,\chi](s) + \mathcal{M}_{22}[\gamma,\chi](s), \tag{28}$$

where (ξ_α is used as an abbreviation for $\xi_\alpha[\gamma, \chi](s)$)

$$\mathcal{M}_{\alpha\beta}[\gamma,\chi](s) = \int_{\mathcal{C}[\gamma,\chi](s)} \xi_\alpha\xi_\beta\,\mathrm{d}A \tag{29}$$

and D and T are defined as

$$D[\gamma, \chi](s) = \int_{\mathcal{C}[\gamma,\chi](s)} \tfrac{1}{2}G[(\partial_s\xi_1)^2 + (\partial_s\xi_2)^2]\,\mathrm{d}A \tag{30}$$

$$T[\gamma, \chi](s) = \int_{\mathcal{C}[\gamma,\chi](s)} G(\xi_2\partial_s\xi_1 - \xi_1\partial_s\xi_2)\,\mathrm{d}A. \tag{31}$$

Here D represents the energy contribution of the change in cross-sectional deformation while T is a term which represents the coupling between the bulk (macrostructural) torsional deformation and the (microstructural) change in cross-section.

4. Approximation scheme

A set of coupled PDEs in the independent variables s and θ is obtained by Lagrange minimizing equation (18) with respect to γ, χ, ψ, $\boldsymbol{r}$ and $\boldsymbol{d}_\alpha$. For reasons of expediency, the PDEs are reduced to ODEs by assuming particular forms for the microstructural degrees of freedom (γ, χ and ψ) motivated by the lowest energy eigenmode of a Cosserat ring. This approximation is discussed in greater depth in appendix B and leads to the following expressions when $(a/R)^2 \ll 1$

$$\gamma(s, \theta) = c_2(s)\mathrm{e}^{\mathrm{i}2\theta} + c_{-2}(s)\,\mathrm{e}^{-\mathrm{i}2\theta} \tag{32}$$

$$\chi(s, \theta) = -\frac{c_2(s)}{2\mathrm{i}}\,\mathrm{e}^{\mathrm{i}2\theta} + \frac{c_{-2}(s)}{2\mathrm{i}}\,\mathrm{e}^{-\mathrm{i}2\theta} \tag{33}$$

$$\psi(s, \theta) = \frac{3c_2(s)}{2\mathrm{i}}\,\mathrm{e}^{\mathrm{i}2\theta} - \frac{3c_{-2}(s)}{2\mathrm{i}}\,\mathrm{e}^{-\mathrm{i}2\theta} \tag{34}$$

where $c_{\pm 2}$ encodes the dominant microstructural deformation. In principle, one can apply boundary conditions (BCs) to the end cross-sections that do not lead to this type of microstructure deformation, but such situations will not be considered here. Microstructure oscillations are generally of much higher frequency than macrostructure oscillations and for the carbon nanotube configurations considered here microstructure eigenmodes of higher frequency than the above are unlikely to be excited significantly. If, for other applications, more general deformations are expected then higher-order modes can be included.

We now substitute equations (32)–(34) into equation (18) to obtain

$$V = \int_0^L \left(\tfrac{1}{2}(\boldsymbol{v}(s) - \boldsymbol{d}_3(s))\boldsymbol{K}(s)(\boldsymbol{v}(s) - \boldsymbol{d}_3(s)) + \tfrac{1}{2}\boldsymbol{u}(s)\boldsymbol{J}(s)\boldsymbol{u}(s) + T(s)\boldsymbol{u}\cdot\boldsymbol{d}_3 + D(s) + U(s)\right)\mathrm{d}s \tag{35}$$

where $\mathcal{A}_0 = 2\pi aR$, $\mathcal{I}_0 = \pi aR^3$ and

$$\mathcal{A}(s) = \mathcal{A}_0 \tag{36}$$

$$\mathcal{I}_{11}(s) = \mathcal{I}_0\left(1 - \tfrac{3}{2}(c_{-2}(s) + c_2(s)) + \tfrac{5}{2}c_{-2}(s)c_2(s)\right) \tag{37}$$

$$\mathcal{I}_{22}(s) = \mathcal{I}_0\left(1 + \tfrac{3}{2}(c_{-2}(s) + c_2(s)) + \tfrac{5}{2}c_{-2}(s)c_2(s)\right) \tag{38}$$

$$\mathcal{I}_{12}(s) = \mathcal{I}_0\tfrac{3}{2}\mathrm{i}\,(c_{-2}(s) - c_2(s)) \tag{39}$$

$$\mathcal{I}_{33}(s) = \mathcal{I}_0\,(2 + 5c_{-2}(s)c_2(s)) \tag{40}$$

$$T(s) = 2\mathrm{i}\mathcal{I}_0 G\left(c_{-2}(s)c_2'(s) - c_2(s)c_{-2}'(s)\right) \tag{41}$$

$$D(s) = \tfrac{5}{2}\mathcal{I}_0 G c_2'(s)c_{-2}'(s) \tag{42}$$

$$U(s) = \tfrac{3}{2}\mathcal{A}_0\frac{a^2}{R^2}Ec_2(s)c_{-2}(s) \tag{43}$$

and $\boldsymbol{K}$ and $\boldsymbol{J}$ take the form of equations (22) and (23).

5. Dimensionless equations

The following dimensionless quantities arise naturally in the above equations: $e = G/E = (2(1+\nu))^{-1}$ (the ratio of the shear modulus to the elastic modulus where ν is the Poisson ratio), $r = R/L$ (the ratio of the cross-sectional radius to the length of the beam), $g = a/R$ (the ratio of the thickness of the cross-section to its radius) and $\bar{s} = s/L$ (the renormalized space variable). Furthermore we will drop the bar over s during the remainder of this paper for ease of reading. We also adopt the shorthand notation $\delta\boldsymbol{v} = \boldsymbol{v} - \hat{\boldsymbol{v}}$.

$$V = EA_0\int_0^1 \tfrac{1}{2}[\delta\boldsymbol{v}\boldsymbol{K}\delta\boldsymbol{v} + g^2U] + \tfrac{1}{2}r^2\left[\tfrac{1}{2}\boldsymbol{u}\boldsymbol{J}\boldsymbol{u} + Tu_3 + \tfrac{1}{2}D\right]\mathrm{d}s \tag{44}$$

where

$$\boldsymbol{K} = (e\boldsymbol{d}_1 \otimes \tilde{\boldsymbol{d}}_1 + e\boldsymbol{d}_2 \otimes \tilde{\boldsymbol{d}}_2 + \boldsymbol{d}_3 \otimes \tilde{\boldsymbol{d}}_3) \tag{45}$$

$$\begin{aligned}\boldsymbol{J} = {} & (1 - 3\Re(c_2) + \tfrac{5}{2}|c_2|^2)\boldsymbol{d}_1 \otimes \tilde{\boldsymbol{d}}_1 + (1 + 3\Re(c_2) + \tfrac{5}{2}|c_2|^2)\boldsymbol{d}_2 \otimes \tilde{\boldsymbol{d}}_2 \\ & + 3\Im(c_2)(\boldsymbol{d}_1 \otimes \tilde{\boldsymbol{d}}_2 + \boldsymbol{d}_2 \otimes \tilde{\boldsymbol{d}}_1) + e(2 + 5|c_2|^2)\boldsymbol{d}_3 \otimes \tilde{\boldsymbol{d}}_3\end{aligned} \tag{46}$$

and

$$U = 3|c_2|^2, \tag{47}$$

$$D = 5e|c_2'|^2, \tag{48}$$

$$T = 4e\Im(c_2^* c_2'). \tag{49}$$

Minimizing the functional $V[\boldsymbol{r}, \boldsymbol{d}_\alpha, c_2]$ leads to

$$\partial_s \boldsymbol{n} = 0 \tag{50}$$

$$\tfrac{1}{2} r^2 \partial_s \boldsymbol{m} + \boldsymbol{v} \times \boldsymbol{n} = 0 \tag{51}$$

$$k_D \partial_{ss} c_2 + k_T (c_2 \partial_s u_3 + 2 u_3 \partial_s c_2) + k_I c_2 + \boldsymbol{u}\boldsymbol{S}\boldsymbol{u} = 0 \tag{52}$$

where $\boldsymbol{n} = \boldsymbol{K}(\boldsymbol{v} - \boldsymbol{d}_3)$, $\boldsymbol{m} = \boldsymbol{J}\boldsymbol{u}$, $k_D = 5e$, $k_T = 4\mathrm{i}e$, $k_I = -12g^2/r^2$ and

$$\boldsymbol{S} = \left(\tfrac{3}{2} - \tfrac{5}{2}c_2\right) \boldsymbol{d}_1 \otimes \tilde{\boldsymbol{d}}_1 + \left(-\tfrac{3}{2} - \tfrac{5}{2}c_2\right) \boldsymbol{d}_2 \otimes \tilde{\boldsymbol{d}}_2 - 5c_2 \boldsymbol{d}_3 \otimes \tilde{\boldsymbol{d}}_3 - \tfrac{3}{2}\mathrm{i}(\boldsymbol{d}_1 \otimes \tilde{\boldsymbol{d}}_2 + \boldsymbol{d}_2 \otimes \tilde{\boldsymbol{d}}_1). \tag{53}$$

6. Perturbative solution

It is possible to find an analytic solution to the standard Cosserat equations through expansion in a perturbation coefficient determined by the deviation of the imposed BCs from the BCs of the reference configuration of the rod. Under such a scheme, solutions can often be found to a controllable level of accuracy. For an example of such an approach, see [2]. At a linear level, such a treatment gives insight into the natural frequency of the structure as well as providing details of the internal behaviour in a convenient analytic form.

For the following analysis we will restrict our BCs to those which keep the torsional component of $\boldsymbol{u}$ (u_3) equal to zero throughout the rod. This reduces the microstructural equations as it allows us to ignore terms depending on u_3 and its derivative.

If we assume that a Cosserat tube is deformed in such a way that the shape of both end cross-sections is circular (i.e. $c_{\pm 2}(0) = c_{\pm 2}(L) = 0$) but each end can be displaced and rotated then the leading order of deformation of the microstructure will be $O(\epsilon^2)$ in the perturbation coefficient ϵ of the BCs (rather than $O(\epsilon)$ for the positions and angles). This can be seen by considering that the source term $\boldsymbol{u}\boldsymbol{S}\boldsymbol{u}$ in equation (52) is quadratic in $\boldsymbol{u}$ (in the case of $u_3 = 0$).

As an example of such a method, we will consider a rod in which the BCs are deformed at one end from their reference configuration by $\epsilon X \boldsymbol{e}_1 + Z\boldsymbol{e}_3$ for the position and $\epsilon \Phi_Y \boldsymbol{e}_2$ for the $SO(3)$ angle vector (corresponding to a rotation of Φ_Y radians around the $\boldsymbol{e}_2$ axis). This means we must find solutions for equations (50)–(52) subject to

$$\boldsymbol{r}(0) = 0, \quad \boldsymbol{r}(1) = \boldsymbol{e}_3 + \epsilon(X\boldsymbol{e}_1 + Z\boldsymbol{e}_3), \tag{54}$$

$$\phi(0) = 0, \quad \phi(1) = \epsilon \Phi_Y \boldsymbol{e}_2, \tag{55}$$

$$c_{\pm 2}(0) = 0, \quad c_{\pm 2}(1) = 0. \tag{56}$$

Note that to leading order in ϵ, $\boldsymbol{r}(s)$ and $\phi(s)$ are the usual solutions to the linearized Cosserat rod equations (i.e. the microstructure has only higher order effect on them). We further assume

that $g^2 \ll r^2$ to facilitate solving (52) for $c_2(s)$. The solutions can be written as polynomials and take the form

$$\boldsymbol{r}(s) = s\boldsymbol{e}_3 + \epsilon \left(\sum_{n=0}^{3} k_{xn} s^n \boldsymbol{e}_1 + k_{z1} s \boldsymbol{e}_3 \right) + O(\epsilon^2) \tag{57}$$

$$\phi(s) = \epsilon \sum_{n=1}^{2} k_{\phi_y n} s^n \boldsymbol{e}_2 + O(\epsilon^2) \tag{58}$$

$$c_2(s) = \epsilon^2 \sum_{n=1}^{4} k_{cn} s^n + O\left(\epsilon^3, \frac{\epsilon^2 g^2}{r^2}\right) \tag{59}$$

where

$$\begin{aligned}
k_{x1} &= d^{-1} 3(\Phi_Y - 2X) r^2 \\
k_{x2} &= d^{-1}(e(3X - \Phi_Y) - 3r^2 \Phi_Y) \\
k_{x3} &= d^{-1} e(\Phi_Y - 2X) \\
k_{z1} &= Z \\
k_{\phi_y 1} &= d^{-1} 2(e(3X - \Phi_Y) - 3r^2 \Phi_Y) \\
k_{\phi_y 2} &= d^{-1} 3e(\Phi_Y - 2X) \\
k_{c1} &= h^{-1}(9e^2 X^2 - (6e^2 + 36er^2)\Phi_Y X + (108r^2 + 3e^2/2)\Phi_Y^2) \\
k_{c2} &= h^{-1}(-27e^2 X^2 + (108er^2 + 18e^2)\Phi_Y X - (36er^2 + 108r^4 - 3e^2)\Phi_Y^2) \\
k_{c3} &= h^{-1}(36e^2 X^2 - (72er^2 + 30e^2)\Phi_Y X + (36er^2 + 6e^2)\Phi_Y^2) \\
k_{c4} &= h^{-1}(-18e^2 X^2 + 18e^2 \Phi_Y X - 9/2 e^2 \Phi_Y^2)
\end{aligned}$$

with $d = e - 6r^2$ and $h = 5d^2$.

This gives us a quick (albeit approximate) method for calculating the microstructural deformation caused by bending the rod. We can further manipulate equations (57)–(59) to reproduce approximations to the localized strain at a given point along the rod and other mechanical properties, as well as allowing us to calculate the potential energy required for such a deformation (and through it the force required at the end of the tube).

Equations (57)–(59) may also prove useful in situations where the microstructure has non-mechanical effects on the system of interest. For example the atomic structure of a carbon nanotube is described using microstructure and so microstructural deformations may change the nanotube's electron transport properties.

Under these circumstances an estimate of the microstructural deformation could be used as a starting point for more complicated atomic methods, or as a way of quickly determining the circumstances under which a nanotube changes its electronic properties.

Reintroducing time t and investigating the model further through a perturbative approach will allow us to investigate microstructural vibrations which may correspond to certain phonon modes in carbon nanotubes (those in which the atomic vibration is radial). It would be interesting to see how closely the classical formula presented within this paper matches the true behaviour of carbon nanotubes and how much less (or even more) accurate it is at simulation compared to so-called *ab initio* techniques such as molecular dynamics and approximate time-dependent density functional theory (DFT) approaches [5]–[7].

Figure 2. Image of a bent tube with $X = 0$, $Z = -0.2$, $\Phi_Y = -0.8$. The tube noticeably deforms at the 'kink'. Here we have set $g = 0$ in order to maximize the microstructural deformation so that it is clearly visible in the image.

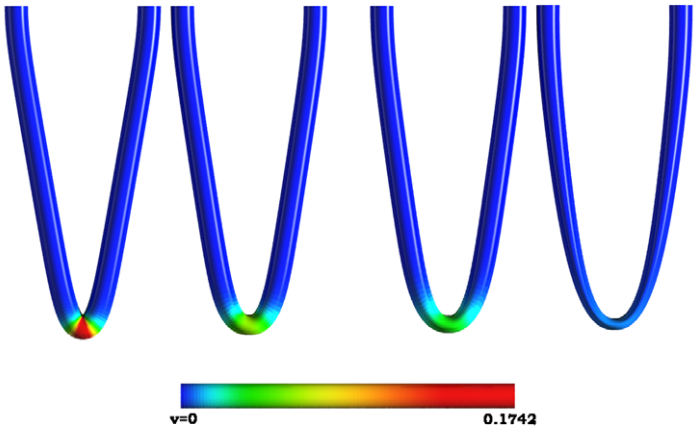

Figure 3. Demonstration of the effect of microstructure on reducing the local strain energy. From left to right we have: no microstructure ($g = \infty$), $g = 0.714$, $g = 0.357$ and $g = 0.0714$. The colour coding indicates the local potential energy $v = (\partial_s V)$. Here the total potential energy of the tube without microstructure is at least 22% greater than with it.

7. Numerical analysis

We have chosen to perform numerical analysis on a system with dimensions and properties similar to a nanotube in order to test the presented theory. Our dimensionless quantities thus become $e = 414\ \text{GPa}/1002\ \text{GPa} = 0.413$, $g = 4.17\ \text{nm}/17.5\ \text{nm} = 0.0238$ and $r = 17.5\ \text{nm}/1000\ \text{nm} = 0.0175$.

Firstly, we present in figure 2 an image of a hollow tube with microstructure generated in POVray[6] from the results of the ODEs. This image is intended to demonstrate the effect of including microstructure. As can be seen, the effect of the microstructure is quite clear and appears to mimic the behaviour of real hollow flexible tubes. This suggests that such a formalism could have uses outside the traditional realm of physics, such as in the visual modelling of hoses for 3D computer-generated imagery (CGI) in games, films, CAD etc.

Let us now compare the effect of increasing the flexibility of the microstructure (by decreasing g). Figure 3 shows a series of tubes with varying g. We have annotated the model of the tubes with the local strain energy $v = (\partial_s V)$. In the case without microstructure, the local strain energy grows extremely quickly in s and maximizes where $\boldsymbol{r}(s)$ has maximum curvature.

[6] Persistence of Vision Pty. Ltd. (2004), *Persistence of Vision Raytracer (Version 3.6)* [Computer software]. Retrieved from http://www.povray.org/download/

As we decrease g however, the maximum local strain energy (found at the centre of the beam) decreases faster than the total potential and all but vanishes (relative to the standard Cosserat rod model) at $g = 0.0714$.

While expected, this behaviour is a typical effect of the microstructure. This result is particularly inspiring as it is known [8] that Nanotubes can be greatly deformed without breaking, a result which could be partly explained by the effect of the microstructure on reducing the local strain energy at the point of maximal bend.

8. Conclusions

In this paper we have presented an extension of the Cosserat model for modelling long, thin, flexible, hollow tubes with microstructural deformations of the cross-sections simulating shell-like behaviour.

Furthermore we have presented an approximation to this microstructure which allows us to reduce a set of two-dimensional PDEs (in the static case) to a set of coupled ODEs. This has advantages over traditional shell theory for both numerical and analytical investigation. In three-dimensional space the presented model results in a set of eight coupled equations.

Through a perturbation technique we have found analytic solutions to these equations which can be considered a good approximation to the true solution for small deviations from the reference state, possibly with a correction to the microstructure provided by numerical analysis. The simple formulae resulting from this analysis could be used as a starting point for more difficult calculations, such as atom dynamics, molecular dynamics and other similar modelling approaches. In the case of nanoscale systems such as nanotubes, the formulae could also be used to determine the position of individual atoms for use in calculations of electron transport properties and other electronic behaviour. We hope to pursue this avenue (with both the perturbative and numerical solutions) in the future.

The analytic approach can also be used to investigate the buckling properties of tubes, such as seen in [9] for nanotubes. Such investigations may predict interesting behaviour which could be further studied by experiments.

Another area of potential interest is in the realm of CGI graphics where the model could provide a basis for generating accurate looking hoses for use in films, games and CAD. Although not investigated here, it is quite possible that a rough approximation can be made to the solutions of the ODEs which will give the correct appearance of the tube under a wide range of deformations. Such an approximation would be very useful for CGI in games where speed of calculation is important while accurate physical behaviour is not.

This model has several areas in which improvements could be made, particularly when it is applied to systems undergoing large deformations from the reference configuration. The most likely cause of error in the presented model is in the energy and shape of the cross-sections. Here we have approximated both the governing equations (through linearization) and the shape (through truncation of the Fourier coefficients and the perturbation series in g^2).

The simplest means for improving the calculation would involve the introduction of more eigenmodes to the Fourier expansion of the cross-section. Likewise the series expansion of the eigenmodes can be extended beyond leading order. At a more advanced level, the governing equations of the cross-sections could be analysed beyond the linear regime to introduce nonlinear corrections to the eigenmodes when deformations are large. Further investigation (whether

experimental, numerical or analytic) would be required to determine the need and applicability of these approximations.

Overall, as a relatively simple formalism, the modelling of Cosserat rods with microstructure could prove a useful and versatile tool for a wide variety of applications. Its ability to deal with changes in the cross-section makes it a worthwhile extension of traditional Cosserat rod theory for the modelling of hollow tubes, particularly beyond linear approximations. While the focus of this paper has been on the modelling of tubes with circular cross-sections (in the reference state), the underlying technique presented can also be applied to any type of variable cross-section for which an energy functional exists.

Appendix A. Cosserat equations on a ring

The motivation for the form of the elastic energy of a Cosserat rod with microstructure uses properties of a closed Cosserat rod constrained to lie in a plane (a Cosserat ring). To avoid excessive notation, many of the symbols introduced in the main body of the paper will now describe properties of a Cosserat ring.

Let $(\boldsymbol{e}_1, \boldsymbol{e}_2, \boldsymbol{e}_3)$ be a basis for a Cartesian coordinate system. The configuration of a Cosserat ring is described by a space curve $\boldsymbol{r}$ and the directors $(\boldsymbol{d}_1, \boldsymbol{d}_2, \boldsymbol{d}_3)$. The reference configuration is a circle of length $L = 2\pi R$ and the reference strains are $\hat{\boldsymbol{v}} = \hat{\boldsymbol{d}}_2$ and $\hat{\boldsymbol{u}} = R^{-1}\hat{\boldsymbol{d}}_3$. The ring lies in the plane with normal $\boldsymbol{e}_3$ and so $\boldsymbol{d}_3 = \hat{\boldsymbol{d}}_3 = \boldsymbol{e}_3$ (note the roles of $\boldsymbol{d}_2$ and $\boldsymbol{d}_3$ are exchanged in comparison with conventional Cosserat rod theory [1]). The cross-sections of the ring are rectangular and have constant width a and constant height h. It follows that the area $\mathcal{A} = ah$ and area moments $\mathcal{I}_{11} = ah^3/12$, $\mathcal{I}_{22} = (ah^3 + a^3h)/12$ and $\mathcal{I}_{33} = a^3h/12$. The elastic modulus E, shear modulus G and density ρ are constant.

The potential energy of the Cosserat ring (assuming the Kirchhoff constitutive relations) is

$$\mathcal{V} = \int_0^L \tfrac{1}{2}[(\boldsymbol{v} - \hat{\boldsymbol{v}}) \cdot \boldsymbol{n} + (\boldsymbol{u} - \hat{\boldsymbol{u}}) \cdot \boldsymbol{m}]\,\mathrm{d}s \tag{A.1}$$

where

$$\boldsymbol{n} = \boldsymbol{K}(\boldsymbol{v} - \hat{\boldsymbol{v}}), \qquad \boldsymbol{m} = \boldsymbol{J}(\boldsymbol{u} - \hat{\boldsymbol{u}}), \tag{A.2}$$

$$\boldsymbol{v} = \partial_s \boldsymbol{r}, \tag{A.3}$$

$$\partial_s \boldsymbol{d}_i = \boldsymbol{u} \times \boldsymbol{d}_i, \tag{A.4}$$

and

$$\boldsymbol{K} = (G\mathcal{A}\boldsymbol{d}_1 \otimes \tilde{\boldsymbol{d}}_1 + E\mathcal{A}\boldsymbol{d}_2 \otimes \tilde{\boldsymbol{d}}_2 + G\mathcal{A}\boldsymbol{d}_3 \otimes \tilde{\boldsymbol{d}}_3), \tag{A.5}$$

$$\boldsymbol{J} = (E\mathcal{I}_{11}\boldsymbol{d}_1 \otimes \tilde{\boldsymbol{d}}_1 + G\mathcal{I}_{22}\boldsymbol{d}_2 \otimes \tilde{\boldsymbol{d}}_2 + E\mathcal{I}_{33}\boldsymbol{d}_3 \otimes \tilde{\boldsymbol{d}}_3), \tag{A.6}$$

$$\boldsymbol{I} = (\mathcal{I}_{11}\boldsymbol{d}_1 \otimes \tilde{\boldsymbol{d}}_1 + \mathcal{I}_{22}\boldsymbol{d}_2 \otimes \tilde{\boldsymbol{d}}_2 + \mathcal{I}_{33}\boldsymbol{d}_3 \otimes \tilde{\boldsymbol{d}}_3). \tag{A.7}$$

If we scale equations (A.1)–(A.4) by changing the variable s to $\theta = s/R$ we can write

$$\mathcal{V} = R^{-2} \int_0^{2\pi} \tfrac{1}{2}[(\boldsymbol{v} - \hat{\boldsymbol{v}}) \cdot \boldsymbol{n} + (\boldsymbol{u} - \hat{\boldsymbol{u}}) \cdot \boldsymbol{m}]\, \mathrm{d}\theta \tag{A.8}$$

where

$$\boldsymbol{n} = \boldsymbol{K}(\boldsymbol{v} - \hat{\boldsymbol{v}}), \qquad \boldsymbol{m} = \boldsymbol{J}(\boldsymbol{u} - \hat{\boldsymbol{u}}), \tag{A.9}$$

$$\boldsymbol{v} = \partial_\theta \boldsymbol{r}, \qquad \partial_\theta \boldsymbol{d}_i = \boldsymbol{u} \times \boldsymbol{d}_i, \tag{A.10}$$

$$\hat{\boldsymbol{v}} = R\boldsymbol{d}_2, \tag{A.11}$$

$$\hat{\boldsymbol{u}} = \boldsymbol{d}_3. \tag{A.12}$$

Let us now set

$$\boldsymbol{r} = R(1 + \gamma(\theta))\hat{\boldsymbol{r}} + R\chi(\theta)\hat{\theta}, \tag{A.13}$$

$$\phi = (\theta + \psi(\theta))\boldsymbol{e}_3, \tag{A.14}$$

$$\hat{\boldsymbol{r}} = \cos(\theta)\boldsymbol{e}_1 + \sin(\theta)\boldsymbol{e}_2, \tag{A.15}$$

$$\hat{\theta} = -\sin(\theta)\boldsymbol{e}_1 + \cos(\theta)\boldsymbol{e}_2. \tag{A.16}$$

Taking derivatives with respect to θ of equations (A.13) and (A.14) gives

$$\boldsymbol{v} = R\hat{\theta} + R(\gamma(\theta) + \partial_\theta \chi(\theta))\hat{\theta} + R(\partial_\theta \gamma(\theta) - \chi(\theta))\hat{\boldsymbol{r}} \tag{A.17}$$

$$\hat{\boldsymbol{v}} = R\cos(\psi(\theta))\hat{\theta} + R\sin(\psi(\theta))\hat{\boldsymbol{r}} \tag{A.18}$$

$$\boldsymbol{u} = (1 + \partial_\theta \psi(\theta))\boldsymbol{e}_3 \tag{A.19}$$

$$\hat{\boldsymbol{u}} = \boldsymbol{e}_3 \tag{A.20}$$

which can be substituted into the energy expression to give

$$\mathcal{V}[\gamma, \chi, \psi] = \pi a R h \int_0^{2\pi} \left(\boldsymbol{y}\boldsymbol{K}\boldsymbol{y} + \frac{a^2 E}{12R^2} (\partial_\theta \psi(\theta))^2 \, \mathrm{d}\theta \right) \tag{A.21}$$

where

$$\boldsymbol{y} = [\partial_\theta \gamma(\theta) - \chi(\theta) + \sin(\psi(\theta))]\hat{\boldsymbol{r}} + [\partial_\theta \chi(\theta) + \gamma(\theta) + 1 - \cos(\psi(\theta))]\hat{\theta} \tag{A.22}$$

$$\boldsymbol{K} = \tfrac{1}{2}(G + E) + \tfrac{1}{2}(G - E)\cos(2\psi(\theta))(\hat{\boldsymbol{r}} \otimes \tilde{\hat{\boldsymbol{r}}} - \hat{\theta} \otimes \tilde{\hat{\theta}}) + \tfrac{1}{2}(G - E)\sin(2\psi(\theta))(\hat{\boldsymbol{r}} \otimes \tilde{\hat{\theta}} + \hat{\theta} \otimes \tilde{\hat{\boldsymbol{r}}}). \tag{A.23}$$

It should be noted that the energy is linear in the height of the ring. This feature is used in the derivation of the energy functional equation (16).

Appendix B. Approximation scheme

Using the results of appendix A, we will derive an approximate expression for the shape of the Cosserat ring.

Let ϵ be an order parameter and replace γ, χ and ψ in equations (A.13) and (A.14) by $\epsilon\gamma$, $\epsilon\chi$ and $\epsilon\psi$. Keeping the leading term in ϵ only in equation (A.21), we have the following potential energy functional:

$$\mathcal{V} = aRhE\epsilon^2 \int_0^{2\pi} \left[e\left(\tfrac{1}{2}(\chi^2 + \psi^2 + (\partial_\theta\gamma)^2) - \chi\psi + \psi\partial_\theta\gamma - \chi\partial_\theta\gamma\right) + \left(\tfrac{1}{2}(\gamma^2 + (\partial_\theta\chi)^2) + \gamma\partial_\theta\chi\right) + \frac{g^2}{12}(\partial_\theta\psi)^2 \right] \mathrm{d}\theta + O(\epsilon^3) \tag{B.1}$$

and since $\hat{\boldsymbol{r}}$, $\hat{\theta}$ and $\boldsymbol{e}_3$ are constant in time t we have the following kinetic energy functional (where $\Phi := R(\chi\hat{\boldsymbol{r}} + \gamma\hat{\theta}) + \xi_\alpha \hat{\boldsymbol{d}}_\alpha(\psi)$):

$$\mathcal{T} = \frac{1}{2}\int \rho(\partial_t\Phi)^2 \,\mathrm{d}A = aR^3h\rho\epsilon^2 \int_0^{2\pi} \frac{1}{2}\left[(\partial_t\chi)^2 + (\partial_t\gamma)^2 + \frac{g^2}{12}(\partial_t\psi)^2\right] \mathrm{d}\theta. \tag{B.2}$$

The Euler–Lagrange equations of motion for γ, χ and ψ generated using the Lagrangian $\mathcal{T} - \mathcal{V}$ are

$$e\partial_\theta f_1 - f_2 = S\partial_{tt}\gamma \tag{B.3}$$

$$ef_1 + \partial_\theta f_2 = S\partial_{tt}\chi \tag{B.4}$$

$$\frac{g^2}{12}\partial_{\theta\theta}\psi - ef_1 = \frac{g^2}{12}S\partial_{tt}\psi \tag{B.5}$$

where $S = R^2\rho/E$, $f_1 = \psi + \partial_\theta\gamma - \chi$ and $f_2 = \gamma + \partial_\theta\chi$.

Since equations (B.3)–(B.5) are linear we can split γ, χ and ψ into Fourier components. Writing the solution as

$$\gamma = \sum_n c_n \exp(\mathrm{i}(n\theta + \Omega_n t)) \tag{B.6}$$

$$\chi = \sum_n q_n \exp(\mathrm{i}(n\theta + \Omega_n t)) \tag{B.7}$$

$$\psi = \sum_n p_n \exp(\mathrm{i}(n\theta + \Omega_n t)) \tag{B.8}$$

we find a series of equations for q_n, p_n and Ω_n which decouple in n as

$$ein(p_n + \mathrm{i}nc_n - q_n) - (c_n + \mathrm{i}nq_n) = \Lambda_n^2 c_n, \qquad e(p_n + \mathrm{i}nc_n - q_n) + \mathrm{i}n(c_n + \mathrm{i}nq_n) = \Lambda_n^2 q_n,$$
$$-g^2n^2p_n - 12e(p_n + \mathrm{i}nc_n - q_n) = g^2\Lambda_n p_n.$$

Little insight is gained from the solutions to the above linear system unless g^2 is small where $p_n = p_n^{(0)} + g^2 p_n^{(2)} + O(g^4)$, $q_n = q_n^{(0)} + g^2 q_n^{(2)} + O(g^4)$ and $\Lambda_n = -S\Omega_n^2 = \Lambda_n^{(0)} + g^2\Lambda_n^{(2)} + O(g^4)$.

Matching the zeroth-order terms we find the lowest-energy eigensolution

$$q_n^{(0)} = \frac{\mathrm{i}c_n}{n}, \tag{B.9}$$

$$p_n^{(0)} = \frac{\mathrm{i}(1-n^2)c_n}{n}, \tag{B.10}$$

$$\Lambda_n^{(0)} = 0 \tag{B.11}$$

and from the second-order terms we find

$$\Lambda_n^{(2)} = -\frac{(n^2-1)^2}{12S(1+n^{-2})} \tag{B.12}$$

so that our leading-order solution is

$$\gamma = \sum_n c_n \exp(\mathrm{i}(n\theta + \Omega_n t)) \tag{B.13}$$

$$\chi \simeq \sum_n \frac{\mathrm{i}c_n}{n} \exp(\mathrm{i}(n\theta + \Omega_n t)) \tag{B.14}$$

$$\psi \simeq \sum_n \frac{\mathrm{i}(1-n^2)c_n}{n} \exp(\mathrm{i}(n\theta + \Omega_n t)) \tag{B.15}$$

where

$$\Omega_n \simeq g\sqrt{\frac{E(n^2-1)^2}{12R^2\rho(1+n^{-2})}}. \tag{B.16}$$

The other two eigenmodes for each n have eigenvalues of $O(1)$ and higher energy than the abovementioned eigenmodes.

In the event of a static deformation of the rod the coefficient c_n determining the contribution of the nth eigenmode will take a value proportional to Ω_n^{-2}. Since Ω_n is approximately proportional to n^2 the contribution will fall off as n^{-4}.

As such, the Fourier coefficients can be truncated at quite a low value of n. For this paper we will keep only the leading $n = 2$ term ($n = 1$ represent translations of the cross-section and can be ignored) as this has approximately eight times the contribution of the $n = 3$ term for 'typical' deformations.

References

[1] Antman S 1991 Non-linear problems in elasticity *Applied Mathematical Sciences* vol 107 (New York: Springer)

[2] Wang C, Liu D, Rosing R, De Masi B and Richardson A 2004 Construction of nonlinear dynamic MEMS component models using Cosserat theory *Analog Integrated Circuits Signal Process.* **40** 117–30

[3] Ru C Q 2000 Effective bending stiffness of carbon nanotubes *Phys. Rev.* B **62** 9973–6

[4] Vodenitcharova T and Zhang L C 2003 Effective wall thickness of a single-walled carbon nanotube *Phys. Rev.* B **68** 165401
[5] Hohenberk P and Kohn W 1964 Inhomogeneous electron gas *Phys. Rev.* B **136** 864–71
[6] Kohn W and Sham L 1965 Self-consistent equations including exchange and correlation effects *Phys. Rev.* A **140** 1133–8
[7] Car R and Parrinello M 1985 Unified approach for molecular dynamics and density-functional theory *Phys. Rev. Lett.* **55** 2471–4
[8] Falvo M R, Clary G J, Taylor R M II, Chi V, Brooks F P Jr, Washburn S and Superfine R 1997 Bending and buckling of carbon nanotubes under large strain *Nature* **389** 582–4
[9] Bower C, Rosen R, Jin L, Han J and Zhou O 1999 Deformation of carbon nanotubes in nanotube-polymer composites *Appl. Phys. Lett.* **74** 3317–9